Electron paramagnetic resonance study of $ZnAl_2S_4$ spinel

2005 J. Phys.: Condens. Matter 17 3943

(http://iopscience.iop.org/0953-8984/17/25/020)

INSTITUTE OF PHYSICS PUBLISHING JOURNAL OF PHYSICS: CONDENSED MATTER

J. Phys.: Condens. Matter **17** (2005) 3943–3952 doi:10.1088/0953-8984/17/25/020

Electron paramagnetic resonance study of $ZnAl_2S_4$ spinel

S Güner[1,4], F Yıldız[2], B Rameev[2,3] and B Aktaş[2]

[1] Physics Department, Fatih University, 34500 Büyükçekmece-Istanbul, Turkey
[2] Gebze Institute of Technology, 41400 Gebze-Kocaeli, Turkey
[3] Kazan Physical-Technical Institute, 420029 Kazan, Tatarstan, Russian Federation

E-mail: sguner@fatih.edu.tr

Received 26 February 2005, in final form 28 February 2005
Published 10 June 2005
Online at stacks.iop.org/JPhysCM/17/3943

Abstract

Single crystals of $ZnAl_2S_4$ spinel doped by paramagnetic Cr^{3+} and Mn^{2+} ions have been studied by the electron paramagnetic resonance (EPR) technique. The crystal field symmetry around the impurity ions has been determined from the angular behaviour of X-band EPR spectra. The anisotropic EPR signal of the Cr^{3+} ions shows splitting into 31 narrow lines due to the super-hyperfine interaction between unpaired electron spins of the chromium centres and nuclear spins of six neighbouring Al^{27} ($I = 5/2$) ions. It has been established that the Cr^{3+} ions are located at the octahedral sites in the spinel structure, and the super-hyperfine interaction results from a weak covalent bounding with the Al atoms. The EPR signals of the Cr^{3+} paramagnetic centres show no fine-structure splitting due to a perfectly cubic symmetry of the local crystal field in the octahedral sites of the $ZnAl_2S_4$ spinel structure. A weak EPR signal consisting of six components has been ascribed to the transitions between hyperfine levels of the Mn^{2+} ($I = 5/2, S = 5/2$) ions located at tetrahedral sites, while the fine-structure splitting of each component could be resolved only for special orientations of the sample in the external magnetic field. The parameters of the EPR signal of both chromium and manganese centres indicate that there is an essential covalence in the $ZnAl_2S_4$ spinel crystal. Very narrow linewidths ($\sim$2 Oe) of the Cr^{3+} EPR signal components point to very high homogeneity and quality of the $ZnAl_2S_4$ crystals.

1. Introduction

The spinels with common formula AB_2O_4 are one of the most important and interesting families of crystalline compounds, having applications in many different areas. Many fascinating

[4] Author to whom any correspondence should be addressed.

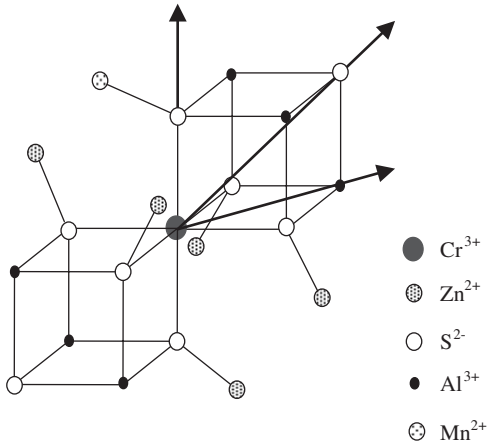

Figure 1. Normal spinel structure of $ZnAl_2S_4$.

properties of these compounds have been observed. For instance, a variety of ferromagnetic and antiferromagnetic properties for a broad range of spinel compositions [1], re-entrant spin-glass and spin-glass-like behaviour in $Cd(Cr_{1-x}In_x)_2S_4$ and $Mn(Cr_{1-x}In_x)_2S_4$ crystals [2, 3], and colossal magnetoresistance in the chalcogenide spinels ACr_2Ch_4 (A = Fe, Cu, Cd; Ch = S, Se, Te) [4] have been observed. Recently there is a rising interest in ferromagnetic semiconductors, such as $CdCr_2Se_4$, $CdCr_2S_4$, $HgCr_2Se_4$, $CuCr_2Se_4$, (see, for instance, [5, 6]). Magnetite ($FeFe_2O_4$), having the spinel structure, has been studied extensively lately because of its half-metallic ferromagnetism that is a very high (almost 100%) spin-polarization of the conduction electrons [7]. Furthermore, the ferromagnetic insulating spinel transition metal oxides (such as $NiFe_2O_4$ and $CoFe_2O_4$) may probably be used as 'spin-filters', which is another approach to create nearly 100% spin-polarization [8]. These unusual properties open up prospects to use the spinel materials in so-called 'spintronic' devices—electronic devices that exploit both the charge and spin of electrons as well as the optical properties of a material [7]. Thus, a new round of research of these materials was stimulated by both recently observed novel physics of spinel compounds and their possible technology applications. The latter are not restricted now by the possibility of use only in solid-state lasers, as forty years ago (although a need in novel laser materials is still a very real task), but are also expanding to a broad range of magnetic, optical, electronic (spintronic) materials and devices.

The $ZnAl_2S_4$ compound crystallizes in the spinel structure with the lattice parameter $a = 10.01$ Å [9]. According to the crystallographic studies, the unit cell belongs to the space group $Fd3m$ (O_h^7) and contains 32 sulfur ions in a cubic close-packed arrangement. There are two cation positions in a perfect spinel lattice: 16 octahedral sites occupied by Al^{3+} ions and 8 tetrahedral sites occupied by Zn^{2+} ions (figure 1). The Cr^{3+} ions are expected to substitute for Al^{3+} ions in the octahedral sites [10]. It is well known that the Cr^{3+} ion plays a very important role in solid-state laser materials. It is an optically active centre in tunable laser materials in the near-infrared spectral region; in addition, it can be used as a sensitizer in rare-earth doped host materials [11–13]. The Cr^{3+} ion is very sensitive to the effect of the host crystal field and its energy spectra vary considerably in various spinel hosts ($ZnAl_2O_4$, $MgAl_2O_4$, $CdIn_2S_4$, etc). It is expected that a relatively small lattice constant should result in a strong crystal field for the Cr^{3+} ions in the octahedral sulfur environment of the $ZnAl_2S_4$ compound [14]. $ZnAl_2S_4$ has an indirect band gap $E_g = 3.42$ eV at room temperature, and the optical

properties of $ZnAl_2S_4$ crystal have been investigated by various techniques (luminescence, photoluminescence, infrared reflectivity, Raman scattering) to explore prospects for possible solid-state laser applications [14–18].

The electron paramagnetic resonance (EPR) technique, which is a very effective method to study the local crystalline and magnetic properties of various systems, has been successfully applied to various spinel crystals as well. For instance, the zero-field splitting parameter (D) of some oxyspinels and sulfospinels has been compared [19]. It has been shown that the observed negative D-value may be understood qualitatively by making a reasonable assumption that the covalent bonding is more pronounced in sulfospinels than in oxyspinels [19]. Moreover, the EPR and optical studies have proved that in the $MgAl_2O_4$ spinel the Cr^{3+} ions, which substitute for Al^{3+}, experience a trigonal crystal field. This field is partly due to a trigonal arrangement of the next-neighbour Al^{3+} ions and partly due to a trigonal distortion of the nearest-neighbour oxygen octahedron [20–23]. A distortion of cubic symmetry on the cation sites has been claimed in the magnetic susceptibility and luminescence studies of the $ZnAl_2S_4$ spinel doped by Cr^{3+} and Cr^{4+} ions substituting for Al^{3+} or two Zn^{2+} ions, respectively [14]. However, to our knowledge, there is no EPR study on the Cr^{3+} doped $ZnAl_2S_4$ compound in the literature to elucidate the local symmetry and crystal field on the octahedral sites as well as the covalence effects in this spinel compound.

Therefore, in this work the EPR technique has been applied to study crystal fields and covalence effects in the Cr-doped $ZnAl_2S_4$ spinel compound. The EPR signals of Cr^{3+} ions and Mn^{2+} (occasional impurity) ions have been observed. For the first time, the super-hyperfine (SHF) interaction of the Cr^{3+} electrons with the neighbouring Al^{27} nuclear spins has been observed in $ZnAl_2S_4$, which gives convincing evidence of an essential covalence of the $ZnAl_2S_4$ crystal.

2. Experimental technique

The Cr-doped $ZnAl_2S_4$ single crystals were grown by a closed tube vapour transport with iodine agent method [16]. The Cr content was estimated from the magnetic susceptibility measurements [14] to be about 0.1 at.%. The orientation of crystal planes was determined by x-ray diffraction measurements. The EPR spectra were recorded by a conventional X-band ($\nu = 9.5$–9.8 GHz) *Bruker EMX* spectrometer employing an AC magnetic modulation (100 kHz) technique. A goniometer was used to rotate the sample with respect to the external magnetic field. An Oxford continuous He gas flow cryostat was used to cool the sample down to the measurement temperature while keeping the microwave cavity at ambient temperature during EPR measurements. The temperature was stabilized by a Lakeshore 340 temperature controller within an accuracy of 1°.

3. Experimental results

Figure 2 shows an experimental EPR spectrum for a particular direction of the external DC field at room temperature. The modulation field amplitude, H_m, is 10 G for this measurement and microwave frequency is 9.53 GHz. As is seen from this figure, there is a strong and relatively broad absorption centred at 3415 G (approximately $g = 1.992$) as well as six relatively weaker peaks (one overlaps the strong peak) with equal intensity and equally separated (approximately 70 G) from each other on both sides of this central peak.

A detailed examination of the strong central peak was done by reducing the modulation field amplitude down to 0.5 G. The EPR spectra were recorded in a narrower field region, which

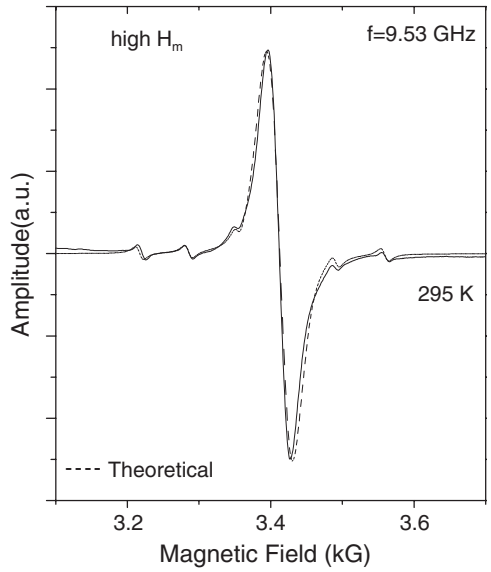

Figure 2. Room-temperature X-band EPR spectrum of the Cr-doped $ZnAl_2S_4$ spinel crystal, $H \parallel [100]$.

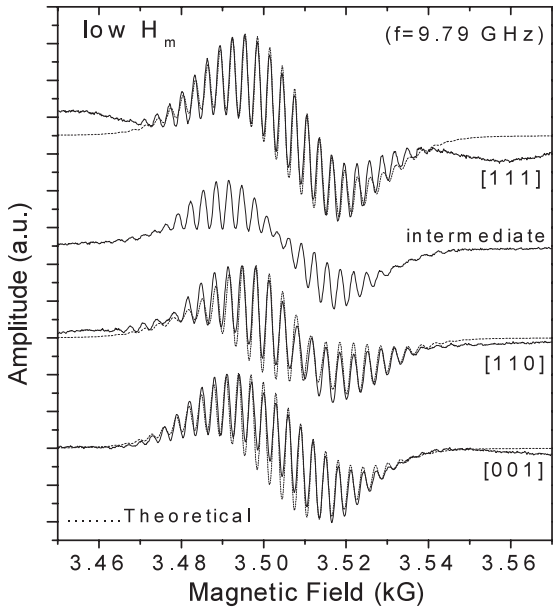

Figure 3. The central multi-line part of experimental EPR spectra of $ZnAl_2S_4$ for various orientations of H in the (110) plane. The simulated super-hyperfine Cr^{3+} spectra for high-symmetry directions are also shown by dashed lines. The simulation parameters are $A_\perp = 3.45$ G and $A_\parallel = 3.00$ G.

is centred at 3510 G in this case due to higher microwave frequency (9.79 GHz). Figure 3 exhibits some experimental EPR spectra for the external magnetic field applied along high-symmetry crystallographic directions. As is seen from figures 2 and 3, there is a dramatic

difference between the spectra recorded using the high and low modulation fields. The strong and broad central absorption line is split into 31 very narrow peaks for lower modulation amplitude. On reducing the modulation field further, it was found that the width of these individual peaks retains its ultimate (minimum) value below $H_m = 0.5$ G corresponding to its intrinsic linewidth.

The spectra in figure 3 exhibit remarkable anisotropic behaviour. As the sample is rotated with respect to the external field in the (110) plane, the overall structure of the spectra changes significantly. The line amplitudes decrease steadily from the spectrum centre towards outer regions for the [100] orientation of the static field, while a more complicated amplitude distribution is observed for the [110] and [111] orientations. There is even exact extinction of the central components of the spectrum for the special directions of the static field, which are intermediate either between [110] and [111], or between [111] and [100] crystalline directions.

The temperature measurements on $ZnAl_2S_4$ crystal were performed in the temperature range 10–300 K. The EPR spectra were recorded for an intermediate direction of external magnetic field with respect to the crystal field axis. There is no noticeable change in the g-factor ($\cong 2$) values of both Cr and Mn EPR signals. The linewidth of the individual components and the distances between the narrow peaks remain almost constant with decreasing temperature.

4. Theoretical analysis

As mentioned above, the six minor peaks in figure 2 on both sides of the main multiplet centred at about 3505 G do not vary significantly with the external field angle with respect to the crystalline axes. This sextet has been attributed to a possible Mn^{2+} impurity, which occurs frequently together with any transition ion like Cr. It should be noted that the Mn^{2+} ion can easily substitute the Zn^{2+} ion at the tetrahedral site of the $ZnAl_2S_4$ spinel due to the very close ionic radii of these ions. Mn^{2+} is an S-state ion ($L = 0$) whose electronic (S) and nuclear (I) spin values are both equal to $5/2$. Thus, each electronic spin state is split into six sublevels due to hyperfine (HF) interaction between S and I that provides the six EPR lines. The sextet of hyperfine Mn^{2+} lines does not show considerable anisotropy, as expected for the Mn ion in a coordination of cubic symmetry. However, one could expect that the six-fold degeneracy of the electronic spin multiplet is lifted due to the effect of the crystalline field. Usually, the fine structure splitting due to the effect of the crystal field (CF) is larger than the hyperfine one. Surprisingly, the magnitude of the fine structure splitting in EPR spectra of the Mn^{2+} ions is so small that the Mn lines nearly overlap, and splitting for three lines has been observed only for special orientations (for the external field applied along [100] or [111] axes of the spinel structure). This indicates a crystal field of cubic symmetry, which is much smaller than the hyperfine interaction but comparable in magnitude with relatively large inherent line-broadening of the individual transitions between $|M_S\rangle$ and $|M_S - 1\rangle$ magnetic states.

On the other hand, the central part of the spectrum containing the 31 narrow peaks can be attributed to the EPR signal from the Cr^{3+} ions substituted for the Al^{3+} ions in the octahedral sites. As is well known, the total orbital (L) and spin angular momentum quantum number (S) of the Cr^{3+} ion are 3 and $3/2$, respectively. The angular momentum is usually expected to quench in a crystalline field giving the orbital energy level distances in the optical frequency range, while the spin multiplet of the Cr^{3+} ion will split in a crystal field with symmetry lower than the cubic one. Therefore, any deviation from cubic symmetry would cause an additional splitting of the spin states, resulting in either line broadening or splitting of the EPR lines. However, the observed nearly symmetrical multi-line structure consisting of 31 components with very small distances between them unambiguously shows that the Cr^{3+} ion multiplet does

exhibit splittings due to SHF interaction rather than the crystal field effect. This reveals almost perfect cubic symmetry around the Cr^{3+} ions substituted at the Al^{3+} sites.

Thus, the anisotropy of the EPR spectra indicates that both Mn^{2+} and Cr^{3+} ions are located at sites of cubic symmetry. The Hamiltonian describing the energy levels of the Cr^{3+} and Mn^{2+} ions can be given as

$$H = H_{\text{Zeeman}} + H_{\text{CF}} + H_{\text{HF}}. \tag{1}$$

Here, the first term represents the Zeeman interaction

$$H_{\text{Zeeman}} = g\beta_{\text{e}} H S = g\beta_{\text{e}}(H_x S_x + H_y S_y + H_z S_z), \tag{2}$$

and the second term represents the crystal field interaction

$$H_{\text{CF}} = B_4(O_4^0 + 5O_4^4), \tag{3}$$

where the coefficient B_4 is usually treated as an empirical parameter to fit the experimental data (in some publications the other form of H_{CF} is used with an equivalent parameter $a = 120B_4$), and O_4^m denotes the Steven's equivalent operators [24]. The crystal field term is zero for Cr^{3+} in the cubic CF by definition due to the low spin value $S = 3/2$. Finally, the third term in equation (1) represents the hyperfine interaction:

$$H_{\text{HF}} = \boldsymbol{S} \cdot \boldsymbol{A} \cdot \boldsymbol{I}, \tag{4}$$

where $\boldsymbol{A}$ is the tensor of hyperfine interaction, while $\boldsymbol{S}$ and $\boldsymbol{I}$ represent electronic and nuclear spin operators, respectively. The isotropic and anisotropic parts of the hyperfine interaction between an electron and a nucleus are respectively given as [25]

$$A_{\text{iso}} = \frac{2\mu_0}{3} g\beta g_{\text{n}}\beta_{\text{n}}|\psi(0)|^2 \tag{5}$$

$$A_{\text{aniso}} = \frac{\mu_0}{4\pi} g\beta g_{\text{n}}\beta_{\text{n}}\langle r^{-3}\rangle, \tag{6}$$

where μ_0, g, g_{n}, β, β_{n}, ψ, and r respectively denote the magnetic permeability of free space, the electronic and nuclear g-factors, the electronic and nuclear Bohr magnetons, amplitude of the electron wavefunction at the nucleus and the average value of the electron radius vector with respect to the paramagnetic ion nucleus. Whereas the isotropic part arises from the Fermi contact interaction, the anisotropic part comes from the dipolar interactions between nuclear (of the paramagnetic centre or neighbouring atom) and electronic spins at the paramagnetic centre. Moreover, in the case of the hyperfine interaction between the electron spins of the Cr^{3+} centres with the nuclear spins of neighbouring ligands, i.e. so-called super-hyperfine (SHF) interaction, there are possible contributions in both the isotropic and anisotropic parts due to covalent hybridization between electron orbitals [26].

No SHF interaction of the Cr^{3+} impurity with the first neighbours (S^{2-} ligands) can be observed in our experiments because of the very small natural abundance (<1%) of the ^{33}S isotope having non-zero nuclear spin. However, a number of the hyperfine components (31) of the Cr^{3+} EPR signal are consistent with the SHF interaction of chromium electrons with 6 nuclei of next-neighbour Al^{3+} ions that impose an essential covalent transfer of unpaired spin through sulfur ligands to the Al atoms [27]. In the simplest model an *isotropic* SHF interaction with a set of equivalent nuclei, each with spin I_i, can be treated as the interaction with one nucleus with a total nuclear spin ${}^{\text{t}}I = \sum_i I_i$ [25]. In fact, using the total nuclear spin for the 6 Al ions, ${}^{\text{t}}I = 6 \cdot \frac{5}{2} = 15$, we obtain the 31 hyperfine lines observed in the experiment. The intensity distribution of hyperfine peaks from left to right in the field for Cr^{3+} ions can be obtained from the coefficients in the expansion of $(1+x+x^2+x^3+\cdots+x^{2I})^n$, where n represents the number of the nearest-neighbouring Al atom with $I = 5/2$ at octahedral sites [25]. However, to describe the experimentally observed *extinction* of the hyperfine lines of the Cr^{3+} EPR spectra for some

orientations the *anisotropic* hyperfine term in our Hamiltonian should be applied, which is in most general form as follows: $H_{HF} = \sum_{i=1}^{6} \boldsymbol{S} \cdot \boldsymbol{A}_i \cdot \boldsymbol{I}_i$. To analyse the experimental spectra we have also done numerical computer simulations, and obtained good results for the high symmetry crystalline directions ([100], [111] and [110]) with the use of axial symmetry of the hyperfine interaction with the principal axis along the line connecting Al and Cr atoms.

5. Discussions

The simulated room-temperature spectra for the Cr^{3+} and Mn^{2+} ions are shown in figures 2 and 3 together with experimental data. Obviously, there is a good agreement between the experimental and the theoretical spectra with respect to both the intensity distribution and the resonance fields for individual peaks. The isotropic contributions to the hyperfine and spectroscopic splitting parameters were deduced as: $A_{Al} = 3.15$ G, $A_{Mn} = 70$ G, $g_{Cr} = 1.992$ and $g_{Mn} = 2.005$.

The fine-structure splitting for the Mn^{2+} ion has been estimated from EPR spectra to be very small (the cubic crystal field parameter $a \sim 5$ G). Splitting into three components observed in experiment for the [100] directions indicates a cubic symmetry of the crystal field. It should be noted that such small cubic crystal fields were also observed in other Mn^{2+}-doped spinel compounds (see [28] and references therein). If the intrinsic linewidth of EPR components is about a few Gauss, they should overlap to give a relatively broad (about 15–20 G) line as observed in our case for most orientations. The resonance fields of the hyperfine peaks for the Mn^{2+} ion show nearly isotropic behaviour. In fact, it is expected that the isotropic part of hyperfine interaction of the manganese electron spin with its own nuclear spin is much stronger than the anisotropic (dipolar) part. Mn^{2+} is an S-state ion with $L = 0$ and the electron cloud of the ion is spherically symmetric around the nucleus. Therefore, a very small value of anisotropic HF interaction for the Mn ion is typically observed in various compounds [28].

The hyperfine parameter of Mn^{2+} ion is significantly smaller compared to its value in any other ionic crystal [29–31]. It is well known [32] that the hyperfine constant A_{Mn} decreases in more covalent crystals. Furthermore, a phenomenological curve was obtained in [33, 34] for the Mn^{2+} hyperfine constant by plotting A_{Mn} versus Pauling's covalence parameter per ligand (c/n). By comparing the experimentally obtained value of 70 G with A_{Mn} in our case one may conclude that this value corresponds to a c/n value of about 18.5%. As the number of ligands at the tetrahedral site is four, the covalence parameter c is 74%. Thus, the magnitude of the hyperfine interaction of the Mn^{2+} signal indicates very high covalence of the $ZnAl_2S_4$ compound. However, additional SHF splitting from the Al nuclear spins, which is observed in the Cr^{3+} signal, is absent in the manganese EPR signal. Apparently the SHF interaction of Mn^{2+} ions with next-neighbour ligands (Al) is very small compared with the linewidth of the Mn^{2+} EPR signal, so an additional structure due to either the crystal field splittings or SHF interaction with the Al ligands could not be resolved. An apparent contradiction between the obtained high covalence of $ZnAl_2S_4$ crystal and small SHF interaction was explained in [34] by the mainly 4s character of bonding to ligands, while the SHF interaction involves a covalent transfer of spin density to ligand through 3d orbitals (see the discussion below). Covalence usually also leads to the reduction of the g-shift, Δg, (i.e. deviation of the g-factor from the free spin value) expected for a purely ionic situation as well. The value of $\Delta g = 0.010$ obtained for the Cr^{3+} signal in the present case should be compared to $\Delta g = 0.022$ reported for MgO: Cr^{3+} or $\Delta g = 0.035$ for Cr^{3+} in fluorides [26, 35]. Therefore, the small Δg value of the Cr^{3+} signal in our case is also consistent with the increase of covalence as expected along the ligand series $F \rightarrow O \rightarrow S$.

The Cr^{3+} EPR spectra show that the isotropic part of the SHF interactions with the Al nuclei is much larger than the anisotropic part. Thereby, rather good results may be obtained

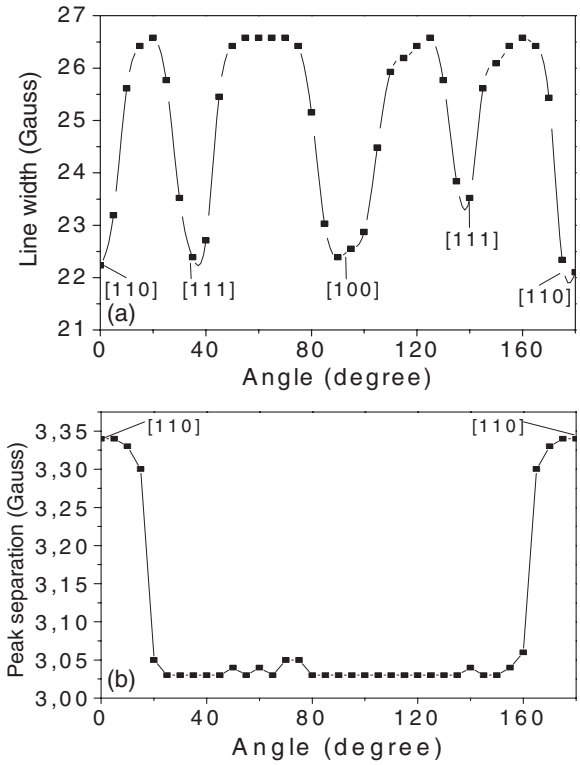

Figure 4. Angular dependence (a) of the linewidth for the envelope curve and separation between the hyperfine peaks (b) of the Cr^{3+} EPR spectra in $ZnAl_2S_4$. The external field is rotated in the (110) plane.

using the simple model of isotropic SHF interactions as outlined above. However, it is possible to estimate the anisotropic contribution to the hyperfine interaction too. For that, the angular dependence of the linewidth of the envelope curve and the successive peak separation within the multiplet for Cr^{3+} ion were plotted in figures 4(a) and (b), respectively. The values vary from 22.20 to 26.60 G for the envelope linewidth and from 3.03 to 3.34 G for the distance of the successive peaks in the multiplet. There is a periodic angular dependence for both curves. It is seen in figure 4 that the envelope linewidth decreases appreciably for the high symmetry directions ([001], [111], and [110]). This fact reflects a small anisotropy of the SHF interaction, which has mainly axial symmetry, and therefore depends on the direction of the DC magnetic field with respect to the line connecting Al and Cr atoms. The 180° symmetry observed for the peak separation of hyperfine peaks is also consistent with an axial symmetry of the anisotropic SHF interaction. In this case, the maximal value of hyperfine tensor is obtained when the DC magnetic field is along the [110] direction, that is along the line to the two (of six) Al^{2+} nearest-neighbour ligands in the $ZnAl_2S_4$ spinel structure.

It is expected [27] that the isotropic contribution in the SHF interaction results from transferring of unpaired spin through (i) π hybridization between the Cr d and S p orbitals and (ii) overlap of S p and Al s orbitals, while a small anisotropic contribution comes mainly from the dipole–dipole interaction with a possible correction due to covalent transfer of the magnetic ion spin onto sulfur ligands. Thus, the isotropic part of the hyperfine interactions with Al^{3+} nuclei is directly proportional to the probability to find the Cr^{3+} magnetic electrons

at the s orbital of the nearest-neighbour Al^{3+} ions. By comparing the value of isotropic part, $A_{Al} = 3.15$ G with the value given in table G. 4 for the s-state electron of the Al atom in [25], we have calculated a probability of $\int |\psi(r)|^2 \, dV \propto P(Al) = 0.0023$ to find the electron at the Al atom. That is, the paramagnetic electrons are localized essentially on the Cr–S orbital with a probability of $P(Cr–S) = 0.9862$.

It is also possible to estimate the contribution in the anisotropic hyperfine interaction due to the dipolar interactions between the magnetic electrons of the Cr^{3+} ion and the Al^{3+} nuclei. The dipolar interaction is inversely proportional to the cube of the distance between the electronic and nuclear spins. Therefore, the anisotropic interaction is expected to be much smaller due to the relatively long distance between Al and Cr ions. Numerical computer simulations with use of axial symmetry of the hyperfine interaction (the simulation parameters are $A_\perp = 3.45$ G and $A_\parallel = 3.00$ G) allow one to estimate a value of anisotropic hyperfine interaction of about 0.45 G. On other hand, using the experimentally observed magnitude of variation in the distance between the hyperfine components we obtain a value of 0.42 G, which is very close to the value estimated from simulation. By using equation (6) and the value of $r_{Cr-Al} = 3.54$ Å obtained from [9], one could estimate the dipolar anisotropic contribution to the A_{Al} value to be about 0.33 G. It is obvious that there is rather good agreement between this value and the experimental ones. Thus, the main contribution to the anisotropic hyperfine interaction comes from the dipole–dipole interaction, while the correction due to covalent transfer is estimated to be about 22%.

Finally, as was mentioned in the previous section, we obtained good agreement with experimental spectra for the high symmetry crystalline directions ([100], [111] and [110]) using the axial symmetry of the hyperfine interaction. However, the simulations show that in order to obtain the extinction of the central components of the spectrum for some intermediate orientations this model has to be complicated further. Probably, a small orthorhombicity of the hyperfine tensor originating from an unpaired spin density in the aluminium 2p orbital (similarly to the results obtained in [26, 27] for the Cr-doped $MgAl_2O_4$ spinel) could account for the observed extinction.

6. Conclusions

Multi-component EPR spectra have been observed in Cr-doped $ZnAl_2S_4$ crystals. The spectra are shown to come from both Cr^{3+} and Mn^{2+} ions. The dominant central part of the spectra belongs to the Cr^{3+} EPR signal and consists of very narrow and equally spaced 31 lines due to super-hyperfine interaction of the Cr^{3+} electron with Al neighbour nuclear spins, while the remaining 6 relatively weaker and broader peaks belong to the Mn^{2+} ion. The theoretical analysis of the experimental data reveals that in the $ZnAl_2S_4$ structure the Mn^{2+} and Cr^{3+} ions substitute for the Zn^{2+} and Al^{3+} ions in the tetrahedral and octahedral ligand coordinations, respectively.

The Mn^{2+} EPR signal reveals a high covalence of the $ZnAl_2S_4$ spinel. The value of the hyperfine constant A for Mn^{2+} corresponds to Pauling's covalence parameter of 74%.

An appreciable covalence of the $ZnAl_2S_4$ crystal has also been confirmed in the analysis of the Cr^{3+} EPR signals. The super-hyperfine structure of the Cr^{3+} spectra shows that there is an essential hybridization between the Cr^{3+} 3d and S^{2-} 2p orbitals with the following transfer of unpaired spin to the Al^{3+} ions. The very small shift ($\Delta g = 0.010$) for the Cr^{3+} ion is consistent with the covalence effect as well.

Very narrow Cr^{3+} lines suggest a high quality and homogeneity of the $ZnAl_2S_4$ crystal and slow relaxation of the Cr^{3+} spins.

References

[1] Chikazumi S 1997 *Physics of Ferromagnetism* (London: Oxford University Press)
[2] Pouget S and Albat M 1995 *J. Phys.: Condens. Matter* **7** 4739–49
[3] Tsurkan V, Baran M, Szymczak R and Szymczak H 1997 *J. Magn. Magn. Mater.* **172** 317
[4] Ramirez A P, Cava R J and Krajewski J 1997 *Nature* **387** 268
[5] Park Y D, Hanbicki A T, Mattson J E and Jonker B T 2002 *Appl. Phys. Lett.* **81** 1471
[6] Unterricker S, Samokhvalov V, Burlakov I, Degering D, Dietrich M, Deicher M and the ISOLDE Collaboration 2001 *Hyperfine Interact.* **136/137** 275
[7] Wolf S A, Awschalom D D, Buhrman R A, Daughton J M, von Molnár S, Roukes M L, Chtchelkanova A Y and Treger D M 2001 *Science* **294** 1488
[8] Szotek Z, Temmerman W M, Svane A, Petit L, Strange P, Stocks G M, Ködderitzsch D, Hergert W and Winter H 2004 *J. Phys.: Condens. Matter* **16** 5587–600
[9] Berthold H J and Kohler K 1981 *Anorg. Z. Chem.* **475** 45
[10] Wyckhoff R W G 1965 *Crystal Structures* vol 3 (New York: Interscience) p 75
[11] Moulton P F, Bass M and Stitch M L 1985 *Laser Handbook* vol 5, pp 203–88
[12] Henderson B and Imbush G F 1988 *Contemp. Phys.* **29** 235
[13] Caird J A, Payne S A, Staver P R, Ramponi A J, Chase L L and Krupke W F 1988 *IEEE J. Quantum Electron.* **24** 1077
[14] Mazurak Z, Cisowski J, Heimann J, Nateprov A and Czaja M 2000 *Chem. Phys.* **254** 25–30
[15] Broussel I, Fortin E, Kulyuk L, Popov S M, Anedda A and Corpino R 1998 *J. Appl. Phys.* **84** 533–40
[16] Broussel I, Fortin E, Kulyuk L and Popov S M 1996 *Solid State Commun.* **99** 921
[17] Kulikova O V, Moldovyan N A, Popov S M, Radautsan S I and Siminel A V 1993 *Japan. J. Appl. Phys.* **32** (Suppl. 32-3) 586–7
[18] Syrbu N N, Bogdanash M and Moldavyan N A 1996 *Infrared Phys. Technol.* **37** 763–8
[19] Henning J C M, Bongers P F, Van Den Boom H and Voermans A B 1969 *Physics* A **30** 307
[20] Atsarkin V A 1963 *Sov. Phys.—JETP* **16** 593
[21] Berger S R 1965 *J. Appl. Phys.* **36** 1048
[22] Stahl-Brada R and Low W 1959 *Phys. Rev.* **116** 561
[23] Wood D L, Imbush G F, Macfarlane R M, Kisliuk P and Larkin D M 1968 *J. Chem. Phys.* **48** 5255
[24] Lea K R, Leask M J and Wolf W P 1962 *J. Phys. Chem. Solids* **23** 1381
[25] Weil J A, Bolton J R and Wertz J E 1994 *Electron Paramagnetic Resonance* (New York: Wiley)
[26] Abragam A and Bleaney B 1970 *EPR of Transition Metal Ions* (Oxford: Oxford University Press)
[27] Bravo D and Böttcher R 1992 *J. Phys.: Condens. Matter* **4** 7295–306
[28] Al'tshuler S A and Kozyrev B M 1974 *Electron Paramagnetic Resonance in Compounds of Transition Elements* 2nd edn (New York: Halsted)
[29] Moreno M 1990 *J. Phys. Chem. Solids* **51** 835–59
[30] Korkmaz M, Dupont M and Aktaş B 1984 *J. Phys. Chem. Solids* **45** 465
[31] Korkmaz M and Aktaş B 1985 *Phys. Status Solidi* b **130** 743
[32] Low W 1957 *Phys. Rev.* **105** 793–80
[33] Matumura O 1959 *J. Phys. Soc. Japan* **14** 108
[34] Šimánek E and Müller K A 1970 *J. Phys. Chem. Solids* **31** 1027–40
[35] Alcala R, Alonso P J, Orera V M and den Hartog H W 1985 *Phys. Rev.* B **32** 4158–63